Assessing the virulence of *Cryptococcus neoformans* causing meningitis in HIV infected and uninfected patients in Vietnam

Lam Tuan Thanh [1], Dena L. Toffaletti [2], Jennifer L. Tenor [2], Charles Giamberardino [2], Gregory D. Sempowski [3], Yohannes Asfaw [4], Hai Trieu Phan [1], Anh Van Duong [1], Trinh Mai Nguyen [1], Guy E. Thwaites [1,5], Philip M. Ashton [1,5], Chau Van Vinh Nguyen [6], Stephen G. Baker [7], John R. Perfect [2], and Jeremy N. Day [1,5]

[1] Oxford University Clinical Research Unit, Wellcome Trust Asia Africa Programme, Ho Chi Minh City, Vietnam

[2] Division of Infectious Diseases, Department of Medicine and Department of Molecular Genetics and Microbiology, Duke University, North Carolina, USA

[3] Duke Human Vaccine Institute and Regional Biocontainment Laboratory, Duke University, North Carolina, USA

[4] Division of Laboratory Animal Resources, Duke University, North Carolina, USA

[5] Centre for Tropical Medicine and Global Health, Nuffield Department of Medicine, University of Oxford, Oxford, UK

[6] Hospital for Tropical Diseases, Ho Chi Minh City, Vietnam

[7] Cambridge Institute of Therapeutic immunology and Infectious Disease, Department of Medicine, University of Cambridge, Cambridge, UK

Correspondence: Jeremy Day: jday@oucru.org Tel : (+84 8) 39237954 Fax : (+84 8) 39238904

Short title: Characterizing *Cryptococcus neoformans* from HIV uninfected patients

Keywords

Cryptococcal meningitis, *Cryptococcus neoformans,* immunocompetent, HIV, virulence

Abstract

We previously observed a substantial burden of cryptococcal meningitis in Vietnam atypically arising in HIV-uninfected individuals. This disease was associated with a single genotype of *Cryptococcus neoformans* (Sequence Type (ST)5), which was significantly less common in HIV-infected individuals. Aiming to compare the phenotypic characteristics of ST5 and non-ST5 *C. neoformans* we selected 30 representative Vietnamese isolates, compared their *in vitro* pathogenic potential and *in vivo* virulence. ST5 and non-ST5 organisms exhibited comparable characteristics with respect to *in vitro* virulence markers including melanin production, replication at 37°C, and growth in cerebrospinal fluid. However, the ST5 isolates had significantly increased variability in cellular and capsular sizing compared with non-ST5 organisms (p<0.001). Counter-intuitively, mice infected with ST5 isolates had significantly longer survival with lower fungal burdens at day 7 than non-ST5 isolates. Notably, ST5 isolates induced significantly greater initial inflammatory responses than non-ST5 strains, measured by TNF-α concentrations (p<0.001). Despite being generally less virulent in the mouse model, we hypothesize that the significant within strain variation seen in ST5 isolates in the tested phenotypes may represent an evolutionary advantage enabling adaptation to novel niches including apparently immunocompetent human hosts.

Introduction

Cryptococcal meningitis (CM) is a life-threatening fungal infection caused principally by *Cryptococcus neoformans* and *Cryptococcus gattii* [1–3]. Despite CM being more common in immunocompromised patients, CM can also arise in apparently immunocompetent patients. Recent figures estimate an annual global CM incidence of 223,100 cases in HIV infected patients, resulting in 181,100 deaths [4].

Generally, *C. gattii* is the most common cause of CM in immunocompetent patients, while *C. neoformans* is primarily responsible for disease in immunocompromised patients [5]. When CM associated with *C. neoformans* var. *grubii* occurs in HIV-uninfected individuals, reports often describe patients with an increased susceptibility due to other underlying immunosuppressive conditions [6,7]. In Vietnam, *C. neoformans* var. *grubii* CM in HIV-uninfected patients accounts for approximately 20% of all CM cases admitted to our hospital in Ho Chi Minh City (HCMC) [8]. We previously reported that the majority of HIV-uninfected CM patients had no identified cause or other medical history suggestive of immunosuppression, and that >80% of HIV-uninfected CM patients were infected by a single genotype of *C. neoformans* var. *grubii* [9], which we later confirmed to be Sequence Type 5 (ST5).

Our clinical observations have been replicated in China, where >70% of CM cases from apparently immunocompetent individuals were infected with *C. neoformans* [10,11]. Again these organisms were latterly identified as genotype ST5 [12,13]. Comparably, ST5 accounted for >80% of HIV-uninfected CM patients in South Korea, although some patients from this location had potentially immunosuppressive conditions [14]. This association between a ST and host immune

phenotype could be explained by lineage-specific increases in pathogenic potential, fitness in the human host, an unidentified host immune deficit, or a combination of these three factors. Recent high-resolution genomic investigation of the population structure of clinical *C. neoformans* var. *grubii* isolates in Vietnam has verified that ST5 and ST4 are genetically distinct lineages of *C. neoformans* var. *grubii*, namely VNIa-5 and VNIa-4 [15].

Here, in order to explore the hypothesis that *C. neoformans* var. *grubii* ST5 have an increased pathogenic potential in comparison to non-ST5 organisms, we compared their *in vitro* virulence phenotypes and exploited an established cryptococcosis mouse model to compare their relative pathogenicity and ability to induce systemic inflammation.

Materials and methods

C. neoformans isolates and culture conditions

We used clinical isolates obtained at the point of diagnosis, prior to antifungal therapy, from the cerebrospinal fluid (CSF) of patients enrolled in a prospective descriptive study of HIV-uninfected patients with central nervous system (CNS) infections, and a randomized controlled trial of antifungal therapy in HIV-infected patients [8,16]. We randomly selected 15 isolates from HIV uninfected CM patients and 15 from HIV-infected CM patients. MLST profiles (CAP59, GPD1, IGS1, LAC1, PLB1, SOD1, URA5) for all isolates were previously determined [17]. *C. neoformans* yeasts were propagated using Yeast Peptone Dextrose (YPD) broth and incubated overnight at 30°C with agitation. Isolates and clinical information from corresponding patients are summarized in Table 1.

Growth at high temperature, in ex vivo human CSF and melanin production

Growth at high temperature and in *ex vivo* human CSF were tested as previously described [18] with modifications for quantitative assessment. To assess fungal growth at different temperatures, the inoculum was adjusted to 10^8 cells/ml, serially diluted and spot-inoculated in duplicate on YPD agar in 5µl aliquots and incubated at 30°C or 37°C for 48 hours. After 48 hours, colony forming units (CFU) were counted and recorded in CFU/ml.

For the *ex vivo* CSF growth assay, baseline pre-antifungal treatment CSF supernatant from random de-identified HIV-infected patients enrolled into an antifungal therapy trial was pooled, filtered, and stored at -80°C until use. 10µl of 10^8 cells/ml yeast suspension was inoculated into 90µl of pooled CSF and incubated at 37°C with 5%CO_2. Inoculated CSF was serially diluted and spotted on YPD agar at days 1 and 3 post-inoculation. All experiments were repeated in triplicate. The H99-derived mutant *Δena1*, which lacks a cation-ATPase-transporter resulting in decreased viability in human CSF and macrophages, was used as a negative control for the *ex vivo* CSF assay [19]. H99 was included as a reference in all experiments. Data were standardized by expressing the results as a ratio of the CFU/ml of the test isolate to the CFU/ml of H99.

Melanin production was assessed by plating 5µl of 10^6cells/mL cell suspension on L-DOPA agar containing 1g/L L-asparagine , 1g/L glucose, 3g/L KH_2PO_4, 250mg/L $MgSO_4.7H_2O$, 1mg/L Thiamine HCl, 5µg/L Biotin, 100mg/L L-DOPA, 20g/L Bacto Agar [20,21]. Plates were incubated in the dark at 30°C or 37°C for 3 days. Differences in colony melanization were compared visually

with reference to H99 and an H99-derived mutant with diminished melaninization in L-DOPA agar from the Perfect lab.

Extracellular urease and phospholipase activity

Extra-cellular urease production was semi-quantified using Christensen's agar. 10µl of 10^8 cells/ml yeast suspension was spotted on Christensen's agar and incubated at room temperature. The time to complete plate colouration was determined using a GoPro Hero 6 camera (Gopro, USA) using the time-lapse setting set with a 1-minute interval. *C. neoformans* H99 was used as a positive control and *Candida albicans* as a negative control. Extracellular phospholipase activity was screened on egg yolk medium as previously described, with minor modifications [22]. The egg yolk medium contained Sabouraud agar with 1M sodium chloride, 0.005M calcium chloride and 8% sterile egg yolk enrichment (Merck, USA). A 5 µl aliquot of *C. neoformans* yeast suspension (10^8 cells/ml) was spotted on egg yolk agar and incubated at 30°C for 72 hours. The diameters of the precipitation zone (D) formed around the colonies and of the respective colonies (d) were recorded after 72 hours incubation. The D/d ratio for each isolate was calculated. H99 was included for reference in each experimental batch. The final result for each isolate was expressed as the ratio between the test isolate's D/d ratio and that of H99. All isolates were tested in triplicate for each phenotype.

In vitro capsule and cell size measurement

To measure *in vitro* cryptococcal capsule thickness, all isolates were streaked onto capsule-inducing agar containing powdered Dulbecco Modified Eagle Medium (DMEM) [supplemented

with 4.5g/L glucose, L-glutamine, sodium pyruvate], $NaHCO_3$ 250mM, NaMOPS 1M, Neomycin 200mg/ml, Cefotaxime 100 mg/ml [23]. Plates were incubated at 37°C in 5% CO_2 until single colonies were visible. Unless otherwise specified, all reagents were purchased from Sigma-Aldrich. India ink smears from a single yeast colony were prepared on a glass slide and visualized at 100X magnification using a CX41 microscope (Olympus, Japan). Images of single microscopic yeast cells were captured using a DP71 Camera system with DP Controller software (Olympus, Japan) and processed using ImageJ (rsb.info.nih.gov/ij/). Capsular thickness was calculated by subtracting yeast cell body diameter (D_{CD}, no capsule) from whole cell diameter (D_{WC}, including capsule). At least 30 individual microscopic yeast cells were assessed for each isolate.

Mouse inhalation infection model of cryptococcosis

All mouse infection experiments were conducted as previously described according to Duke University's Institutional Animal Care and Use Committee guidelines and approvals [24]. Six-week old female A/J mice were sedated with isoflurane and inoculated intranasally with the selected *C. neoformans* var. *grubii* isolate by dropping 25µl of yeast suspension containing $5x10^4$ cells into the nares. Eight isolates were randomly selected from the 30 for murine experiments. The isolates were five ST5 (BK147 and BK44 from HIV infected patients and BMD700, BMD1338 and BMD1646 from HIV uninfected patients) and three non-ST5 strains (BMD1415 (ST4) and BMD1367 (ST306) from HIV uninfected patients and BK80 (ST4) from an HIV infected patient). Animals were monitored daily and euthanized by CO_2 inhalation at indicated time points (fungal

155 burden and *in vivo* responses) or until weight loss ≥ 15% body weight was observed (virulence
156 assay).
157
158 *Determining in vivo fungal burden*
159 Five mice were infected with each isolate in two independent experiments for assessment of
160 fungal burden at 7- or 14-days post-infection. All animals in each experiment set were
161 euthanized by CO_2 inhalation either on day 7 or day 14 post-infection. Fungal burden at each
162 time point was assessed by excising the left superior lobe of the lung and brain and
163 homogenizing the tissue by bead beating. Tissue homogenate was serially diluted and plated
164 onto YPD agar supplemented with 100mg/ml ampicillin. The plates were incubated at 30°C for
165 48 hours and the number of *C. neoformans* colony forming units (CFU) recorded. Fungal
166 burdens were expressed as CFU per gram of tissue (CFU/g). At each time point, additional lung
167 lobes were also collected for determining *in vivo* histopathology and cytokine response, as
168 described below. In addition, fungal burdens were separately determined at the point of death
169 in animals from the survival assays described below.
170
171 *Determining in vivo histopathology*
172 At specific time points (7 or 14 days post-infection, as described above), the right superior lung
173 lobe from each mouse was excised and immersed in 10% formalin (replaced with 70% ethanol
174 after 24 hours) for fixation. Fixed, uninflated lung specimens were stored at 4°C until further
175 processing. After paraffin embedding, sliced sections were stained using the periodic acid-Schiff
176 (PAS) or mucicarmine stains. Histopathological examination was performed by an independent

177 pathologist blinded to infecting strain. Tissue damage was scored from 0 (no changes) to 10
178 (severe changes), corresponding to the severity of pathology in 4 different categories: necrosis,
179 hemorrhage, edema and inflammation, as per the Duke Veterinary Diagnostic Laboratory
180 (Division of Laboratory Animal Resources).
181
182 *Determining in vivo cytokine response*
183 To assess the severity of the inflammatory responses at specific time points (day 7 and day 14
184 post-infection), the middle lobe from the right lung of each infected mouse was excised and
185 homogenized by bead beating in 1ml sterile PBS/Protease inhibitor. 500µl of lung homogenate
186 was used for cytokine profiling. Cytokines representing T-helper type 1 (Th1) (IL-12p70, TNF-α,
187 IFN-γ), T-helper type 17 (IL-17) and T-helper type 2 (Th2) (IL-4, IL-5, IL-10) responses were
188 measured using a customized Bio-Plex Pro™ Mouse Cytokine Th1/Th2 Assay kit (Biorad, USA)
189 with the BioPlex 200 platform according to the manufacturer's guidelines. Data were retrieved
190 using BioPlex Manager Software. The upper and lower limits of quantification (ULOQ and LLOQ)
191 were based on a standard curve. All values falling below the LLOQ were replaced with the
192 midpoint between zero and the LLOQ. Data were standardized by lung weight and presented as
193 picogram of cytokines per gram lung tissue (pg/g).
194
195 *In vivo virulence assay*
196 The virulence assay was conducted independently from the day 7/day 14 experiment. Each of
197 the 8 selected isolates was inoculated intranasally into 10 A/J mice. Mice were monitored daily

until death, or loss of more than 15% body weight (impending death), at which point they were euthanized by CO_2 inhalation, necropsied and had fungal burden in lung and brain determined.

Statistical analysis

GraphPad Prism version 5.04 for Windows (GraphPad Software, San Diego California USA; www.graphpad.com) was used for data visualization and statistical analyses of fungal loads, cytokine profiling, capsular/cell size, and survival proportions. The Mann-Whitney U-test was used for comparing fungal load and cytokine concentrations. Kaplan-Meier survival curves and the log-rank test were used for survival analysis. Capsule/cell size was compared using Welch's t-test. The Fligner-Killeen test of variance homogeneity for analyzing variation in capsule/cell size and Fisher's exact test were performed using R software, version 3.2.4 (http://www.r-project.org). One way ANOVA with post hoc multiple comparison tests (Dunnett or Bonferroni) was used to compare cytokine concentrations between individual isolates.

Results

C. neoformans in vitro virulence

We compared the capsule size, extracellular urease, phospholipase production, melanin production, growth at high temperature, and growth in pooled human CSF between the 15 ST5 and the 15 non-ST5 *C. neoformans* isolates. We observed no significant genotype-specific differences between growth at 30°C (p=0.10), growth at 37°C (p=0.23), *ex vivo* survival in CSF after 1-day (p=0.72), *ex vivo* survival in CSF after 3-days of exposure (p=0.77), extracellular urease activity, or phospholipase activity (Figure S1). ST5 *C. neoformans* cells developed

220 significantly thicker capsules during *in vitro* culture than non-ST5 isolates (Table 2). Individual
221 ST5 *C. neoformans* cells were also significantly larger than non-ST5 cells (Figure 1), and we
222 observed significantly greater variation in capsule size and cell diameter within ST5 cells than
223 non-ST5 cells (Figure 1; $p<0.0001$, Fligner-Killeen test). Notably, a single organism (BMD1646),
224 was clearly larger and with thicker capsules than other isolates. However, the difference in
225 capsule thickness and cell diameter between STs remained statistically significant even when
226 this isolate was removed from analysis.
227
228 *In vivo mouse infections with ST5 and non-ST5 isolates*
229 We hypothesized that a higher prevalence of ST5 infections in apparently healthy hosts was
230 associated with higher virulence. Therefore, we challenged A/J with equivalent doses of
231 representative isolates (5 ST5 and 3 non-ST5; the individual *in vitro* virulence phenotyping
232 results for these 8 isolates are presented in supplementary Figures S2-S4). Contrary to our
233 hypothesis, we found that mice infected with ST5 organisms had significantly longer survival
234 times than mice infected with non-ST5 organisms ($p<0.0001$, Figure 2A). However, there was
235 significant variability in the effect of individual organisms of the same ST on survival (Figure 2B).
236 Specifically, two ST5 organisms (BK147 and BMD1646) were substantially attenuated in
237 comparison to other ST5 organisms; the mice infected with these organisms survived up to 40
238 days. However, differences in survival times between mice infected with ST5 and non-ST5
239 organisms remained significant when these two isolates were removed from the analysis
240 ($p=0.003$; log-rank test).
241

The tissue-specific fungal burden data are shown in Table 3. All organisms established lung infection and disseminated brain infection as early as 7 days post infection. Non-ST5 infections resulted in higher fungal burdens in lung than ST5 infections at all time-points (day 7, $p<0.001$; day 14, $p<0.0001$; and end of the experiment, $p<0.0001$ (Figure 3). Again, these data were not driven by the two apparently attenuated ST5 isolates as the fungal loads associated with the ST5 infections were significantly lower even when excluded from the analysis. The majority of animals infected with the attenuated ST5 organisms (BMD1646 (4/5 mice) and BK147 (5/5 mice)) had low fungal burdens in the lungs up to day 14 (Figure 3). Fungal burdens in the brain were higher in non-ST5 infected animals at all time points; however, this difference was only statistically significant at the end of the experiment ($p=0.054$, $p=0.36$, and $p=0.01$; Mann-Whitney test at days 7, 14 and point of impending death (time when 15% body weight loss is observed).

ST5 C. neoformans isolates induce of TNF-α in the lungs of infected mice

We next measured the cytokine concentrations in lung homogenates at days 7 and 14 post-infection (Figure 4). The concentrations of TNF-α were significantly higher in lung homogenates from mice infected with ST5 than non-ST5 infections ($p=0.01$). Of note, the highest day 7 lung TNF-α concentrations were associated with the ST5 organisms that were most attenuated in the mouse survival model (BK147 and BMD1646). Correspondingly, the lowest TNF-α concentrations were measured in the most virulent ST5 isolate in the mouse model (BMD1338).

263 By day 14, the mean TNF-α concentrations in lung homogenates associated with the ST5
264 infections had declined from 3933.71 pg/g lung to 2802.36 pg/g lung (p<0.001). Other Th-1
265 cytokines including IL-12, IL-17, and IFN-γ also decreased in ST5-infected mice between days 7
266 and 14 (p<0.001, p<0.01 and p=0.02, respectively). This contrasted with the non-ST5 infections,
267 in which the mean TNF-α levels had increased from 3256.25 pg/g to 6378.76 pg/g (p=0.02) over
268 this same period. The high TNF-α concentration associated with non-ST5 infections at day 14
269 was driven by a single isolate - BMD1415. The TNF-α concentrations in in lung homogenates
270 from mice infected with this isolate were significantly higher than for infections with any other
271 isolate of any lineage (p<0.001). There was no statistically significant differences in TNF-α
272 concentrations at day 14 between lineages when this isolate was excluded from the analysis.
273 Similarly, the concentrations of these two cytokines in BMD1415-infected mice was significantly
274 higher than in mice infected with any other isolate (p<0.001). However, the IL-12
275 concentrations declined in non-ST5-infected mice, including BMD1415, between day 7 and 14
276 (4 fold decrease, p<0.0001) (Figure 5).
277
278 We measured the TNF-α:IL-10 ratio as a proxy for the relationship between a Th-1 and a Th-2
279 response [25]. From day 7 to day 14 days post-infection, the TNF-α:IL-10 ratio decreased by a
280 factor of 0.78 in mice infected with ST5 isolates, while those infected with non-ST5 strains
281 exhibited an increase in the ratio of 1.25-fold. However, when BMD1415 (ST4) was excluded
282 from the analysis the TNF-α/IL-10 ratio in non-ST5 infected mice decreased by a factor of 0.67.
283 By day 14 we detected elevated concentrations of IL-17 and IFN-γ in non-ST5 infected mice (5-
284 fold and 17-fold increments, respectively (Table 4), but not in ST5 infected mice. Again, this

effect was largely associated with BMD1415, since the concentrations of IL-17 and IFN-γ induced by this isolate at day 14 were significantly higher than for all others (p<0.001).

Histopathological examination

Histological examination of infected lung tissue revealed evidence of inflammation, hemorrhage, edema and necrosis in most cases. These changes were generally greater by day 14 in comparison to day 7. There were no clear differences in histological scores between ST, other than with BMD1646 (ST5) which generated only mild inflammation with no evidence of necrosis or hemorrhage (Figure S5). PAS staining revealed extensive perivascular infiltration of leukocytes in mice tissue associated with both infecting genotypes (BMD1338-ST5 and BMD1415-ST4, Figure 6). Extensive *in vivo* encapsulation of *C. neoformans* var. *grubii* in mouse lung was visualized using Mucicarmine staining (Figure 7). However, it was unknown whether the bigger capsule and cell size associated with ST5 organisms *in vitro*, as described earlier, was also evident *in vivo* since we were unable to perform this measurement.

Discussion

Most cases of cryptococcal meningitis in HIV uninfected, apparently immunocompetent, patients in Vietnam and East Asia are due to *C. neoformans* strains of multi-locus sequence type 5 (ST5) [9,10,12,17,26–28]. This phenomenon could be explained either by ST5 strains being intrinsically more pathogenic, or due to unidentified lineage–specific host immune defects or exposures. It is unlikely that the high prevalence of ST5 infection observed in HIV-uninfected patients is explained by a significantly greater prevalence of the lineage in the environment

since it causes only 35% of cases in HIV-infected patients within the same geographical area [9]. Furthermore, data from China suggest that ST5 strains are significantly less prevalent in the environment, making up only 5% of isolates recovered in a recent study [29]. We investigated the first hypothesis by comparing previously identified *in vitro* virulence-associated phenotypes, along with murine *in vivo* virulence and immune responses, between lineages. All isolates were derived from HIV infected or uninfected Vietnamese patients with cryptococcal meningitis. The comparison by MLST defined lineage is appropriate because ST5 is a coherent and distinct group, whole genome sequence data revealing that there are few intra-lineage genomic variations between ST5 strains [17]. More recent phylogenetic analysis using whole genome sequencing of a larger collection of clinical isolates from Vietnam, including the eight strains tested in the mouse model, has established that the MLST ST5 and ST4/ST6/306 groups are genetically distinct lineages (VNIa-5 and VNIa-4, respectively) [15]. It is unlikely that any phenotypic variations among ST5 isolates are primarily attributable to *subtle* intra-lineage genomic variations since phenotypic and genotypic diversity are not tightly coupled in *C. neoformans* var. *grubii* [30]. Due to the fact that ST5 has been shown to be consistently associated with the clinical phenotype of interest (infection in HIV-uninfected patients), and that strains from HIV uninfected patients are dispersed throughout the VNIa-5 cluster, we believe the ability to infect apparently immunocompetent hosts is common to all ST5 isolates. All comparisons of ST versus non-ST5 in this study were thus essentially VNIa-5 versus VNIa-4. We found that isolates from all STs were able to grow in *ex vivo* human CSF and at 37°C - essential characteristics for establishing human CNS infection. While these qualities would be needed for disease in both HIV infected and immunocompetent patients, it might have been

329 expected that ST5 strains would grow more rapidly in these conditions. The lack of ST-specific
330 differences in these phenotypes suggests that the ability to establish disease in HIV-
331 uninfected/immunocompetent patients is not driven by simple adaptations to these conditions.
332 Noticeably, ST5 cells were significantly larger than non-ST5 cells, had thicker capsules *in vitro*,
333 and had more within lineage variation in these characteristics. Capsule size and composition are
334 known to vary during infection and under specific stress conditions [31,32], influencing
335 macrophage phagocytosis and modulating host immune response [32–35], and in human disease,
336 *ex vivo* capsule size has been associated with higher intracranial pressures, slower yeast
337 clearance and attenuated inflammation [34].While we did not formally measure yeast cell or
338 capsule size in our *in vivo* experiments, mucicarmine staining was suggestive that capsules were
339 indeed larger during mouse infection. It is possible that the ability of ST5 strains to cause
340 infections in immunocompetent patients is a function of increased responsiveness to capsule-
341 inducing conditions. Further investigation of genotype-specific characteristics of *in vitro* and *in*
342 *vivo* capsular polysaccharide production, composition, and morphology, may elucidate a
343 specific role in ST5-associated pathogenesis. Of note, cryptococcal virulence factors frequently
344 have additional metabolic functions; the increased cell and capsule size seen in ST5 isolates
345 may be a side effect of other processes involving capsular-biosynthesis genes (for example
346 carbon source sensing, sugar transport and spore formation) [36,37].
347 Our data indicate that phenotypic heterogeneity may be a hallmark characteristic of the ST5
348 lineage. Heterogeneity is a desirable trait for microbial populations under selection pressure
349 allowing the exploitation of, and survival, in novel niches [38]. Chow *et al* (2008) has previously
350 reported that ST5 *C. neoformans* var. *grubii* possesses unique genomic features which may

drive niche adaptation [39]. We speculate that the phenotypic heterogeneity associated with strains from the ST5 lineage is a strategy that facilitates successful colonization of novel environmental niches, including the exploitation of infrequent specific human immune deficits. Morphological variation including cell size, capsule size and cell shape has also been associated with different patient clinical symptoms, suggesting greater capacity for pathogenicity, immune evasion and pathogenesis [40].

However, paradoxically, we found no evidence that ST5 isolates have greater virulence in the mouse model. There are several possible explanations. First, virulence in mice is variable depending on mouse breed and may not accurately reflect the immunological heterogeneity of the human population [41]. Second, yeasts with different pathogenic potentials, associated with their isolation from different sources (i.e. clinical versus environmental, immunocompromised versus immunocompetent patients) may have the same or paradoxical pathogenic potential in experimental animal models. An example is *Cryptococcus gattii* which is associated with infection in immunocompetent patients and therefore is considered to be more fit in the human host than *C. neoformans*. However, the hypervirulent *C. gattii* strain R265, responsible for the on-going Vancouver outbreak, has similar virulence in both C57BL/6 and A/J mice to the *C. neoformans* H99 strain, which was derived from a patient with Hodgkin's disease on chemotherapy [42]. Third, the A/J mouse breed is not immunologically intact; it may be an imperfect model of infection for immunocompetent hosts [43]. Rather, A/J mice may be a better model of disease in immunosuppressed patients, as they are highly susceptible to cryptococcal disease, and the patterns of cytokine expression in mice with disseminated cryptococcosis are similar to those seen in HIV-infected patients with CM [44]. Consistent with this, we could not

373 detect clinical differences in disease course or outcome between HIV patients infected with ST5
374 versus other strains in Vietnam [17]. Models that better mimic infection in immunocompetent
375 hosts are needed.
376 We did identify lineage specific differences in immune response in the mouse model. Previous
377 research has suggested that a Th1 type immune response, defined by the TNF-α/IL-10 ratio, is
378 protective, and a Th2 response is associated with poor outcomes [45,46]. We found no evidence of
379 genotype-specific differences in TNF-α/IL-10 ratios by lineage in the murine infection model.
380 Rather, we found higher initial (day 7) TNF-α concentrations in mice infected with ST5 isolates,
381 suggesting this genotype elicits a more intense initial inflammatory response. Previous studies
382 have suggested that capsule components, or cryptococcal cells themselves, have a dose-
383 dependent ability to stimulate TNF-α production by various immune effector cells [47,48]. The
384 more robust initial inflammatory response we observed may have been due to the ST5 capsular
385 phenotype. Previously, it has been suggested that the ability of *C. gattii* to cause disease in
386 apparently immunocompetent patients is because it induces a less severe inflammatory
387 response compared with other cryptococcal species [42]. The robust initial inflammatory
388 responses seen in our murine infection experiments are not consistent with this being the
389 mechanism underlying the ability of ST5 *C. neoformans* var. *grubii* organisms to cause disease in
390 the immunocompetent.
391 *In vivo* controlled infection studies in mice, including ours, commonly employ the classic
392 definition of pathogenicity as the microbe's capability to cause disease in a susceptible host,
393 whereas virulence corresponds to the severity of the ensuing pathology [49]. Using the same
394 infective dose for all strains we failed to demonstrate that ST5 strains had greater virulence.

The difference we observe in prevalence of different lineages in immunocompetent and immunosuppressed humans may actually represent specific differences in pathogenicity - the ability of the organisms to colonize the host and establish infection. We could not assess this with our experimental system.

In summary, our cohort of ST5 *Cryptococcus* isolates displayed two notable phenotypes. First, despite their well-documented ability to cause disease in HIV uninfected humans, they appeared to be less virulent in a murine model than the other sequence types, as demonstrated by reduced fungal burdens in tissue and prolonged mouse survival. Second, ST5 strains had larger capsules and cell sizes than the other genotypes, and greater variability in this phenotype throughout the lineage. These data lead us to the following conclusions. First, clinical isolates, which have by their nature already undergone selection within the human host, can possess wide variability in the expression of virulence phenotypes within a single lineage. Secondly, the use of host risk factors and immune phenotypes to derive an understanding of the factors that drive the pathogenicity of *Cryptococcus neoformans* may be more complex than anticipated. Associations may be difficult to make due to the relevance of the particular *in vitro* phenotypes, the animal models used, within strain heterogeneity, and population substructure. Moreover, there may be heterogeneity in the immune response of apparently immunocompetent patients which selects particular sub-cohorts of isolates of the same lineage. Laboratory phenotyping of larger numbers of clinical isolates is needed to define the lineage-specific differences that determine different human disease phenotypes.

Finally, it is possible that the categorization of strains into specific clades with limited genetic information such as MLST may lack precision to understand the relative fitness of specific

417 strains in the human host. It is likely that whole genome sequencing will provide better
418 mapping of the relationships between strains and virulence.
419 In conclusion, in this study, we demonstrated genotype-specific differences in *in vitro* and *in*
420 *vivo* virulence phenotypes between *C. neoformans* var. *grubii* strains isolated from host with
421 different immune status. However, there was also significant variation among strains isolated
422 from apparently immunocompetent patients in specific *in vitro* and *in vivo* phenotypes tested.
423 This higher rate of phenotypic variation may represent an evolutionary strategy for *C.*
424 *neoformans* var. *grubii* to take advantage of novel niches and contribute to their ability to infect
425 apparently immunocompetent hosts, despite generally being less virulent in a mammalian
426 animal model. Furthering the understanding of the pathogenesis of cryptococcal meningitis will
427 require investigation of large numbers of strains with associated robust clinical information,
428 and the development of high throughput laboratory phenotypic studies that have clinical
429 relevance in humans.

430 **Acknowledgements**

431 This work was supported by a Wellcome Trust Intermediate Fellowship awarded to JND
432 (WT097147MA), and a Henry Dale Fellowship jointly funded by the Wellcome Trust and the
433 Royal Society (100087/Z/12/Z) awarded to SGB. Multiplex cytokine profiling was performed in
434 the Immunology Unit of the Duke Regional Biocontainment Laboratory, which received partial
435 support for construction from the US National Institutes of Health, National Institute of Allergy
436 and Infectious Diseases (UC6-AI058607). The study was approved by the scientific committee of
437 the Hospital for Tropical Diseases, Ho Chi Minh City, Vietnam.

438

Conflicts of Interest

None

References

1. Fang W, Chen M, Liu J, et al. Cryptococcal meningitis in systemic lupus erythematosus patients: pooled analysis and systematic review. *Emerg Microbes Infect*. 2016;5(9):e95. doi:10.1038/emi.2016.93

2. Schmalzle SA, Buchwald UK, Gilliam BL, Riedel DJ. *Cryptococcus neoformans* infection in malignancy. *Mycoses*. 2016;59(9):542-552. doi:10.1111/myc.12496

3. Williamson PR, Jarvis JN, Panackal AA, et al. Cryptococcal meningitis: epidemiology, immunology, diagnosis and therapy. *Nat Rev Neurol*. 2016;13(1):13-24. doi:10.1038/nrneurol.2016.167

4. Rajasingham R, Smith RM, Park BJ, et al. Global burden of disease of HIV-associated cryptococcal meningitis: an updated analysis. *Lancet Infect Dis*. 2017;17(8):873-881. doi:10.1016/S1473-3099(17)30243-8

5. Kwon-Chung KJ, Fraser JA, Doering TL, et al. *Cryptococcus neoformans* and *Cryptococcus gattii*, the etiologic agents of cryptococcosis. *Cold Spring Harb Perspect Med*. 2014;4(7):a019760. doi:10.1101/cshperspect.a019760

6. Pappas PG. Cryptococcal infections in non-HIV-infected patients. *Trans Am Clin Climatol Assoc*. 2013;124:61-79.

7. Shih CC, Chen YC, Chang SC, Luh KT, Hsieh WC. Cryptococcal meningitis in non-HIV-infected patients. *QJM*. 2000;93(4):245-251. doi:10.1093/qjmed/93.4.245

8. Chau TT, Mai NH, Phu NH, et al. A prospective descriptive study of cryptococcal meningitis in HIV uninfected patients in Vietnam - high prevalence of *Cryptococcus neoformans* var. grubii in the absence of underlying disease. *BMC Infect Dis*. 2010;10(1):199. doi:10.1186/1471-2334-10-199

9. Day JN, Hoang TN, Duong A V, et al. Most cases of cryptococcal meningitis in HIV-uninfected patients in Vietnam are due to a distinct amplified fragment length polymorphism-defined cluster of *Cryptococcus neoformans* var. grubii VN1. *J Clin Microbiol*. 2011;49(2):658-664. doi:10.1128/JCM.01985-10

10. Chen J, Varma A, Diaz M. *Cryptococcus neoformans* strains and infection in apparently immunocompetent patients, China. *Emerg Infect Dis*. 2008;14(5).

11. Li Z, Liu Y, Cao H, Huang S, Long M. Epidemiology and clinical characteristics of cryptococcal meningitis in china (1981-2013): A review of the literature. *Med Mycol Open Access*. 2017;3(1):1-6. doi:10.4172/2471-8521.100022

12. Fan X, Xiao M, Chen S-L, et al. Predominance of *Cryptococcus neoformans* var. *grubii* multilocus sequence type 5 and emergence of isolates with non-wild-type minimum inhibitory concentrations to fluconazole: a multi-centre study in China. *Clin Microbiol Infect*. 2016;22(10):887.e1-887.e9. doi:10.1016/j.cmi.2016.07.008

13. Dou H-T, Xu Y-C, Wang H-Z, Li T-S. Molecular epidemiology of *Cryptococcus neoformans* and *Cryptococcus gattii* in China between 2007 and 2013 using multilocus sequence typing and the DiversiLab system. *Eur J Clin Microbiol Infect Dis*. 2015;34(4):753-762. doi:10.1007/s10096-014-2289-2

14. Choi YH, Ngamskulrungroj P, Varma A, et al. Prevalence of the VNIc genotype of

Cryptococcus neoformans in non-HIV-associated cryptococcosis in the Republic of Korea. *FEMS Yeast Res*. 2010;10(6):769-778. doi:10.1111/j.1567-1364.2010.00648.x

15. Ashton PM, Thanh LT, Trieu PH, et al. Three phylogenetic groups have driven the recent population expansion of *Cryptococcus neoformans*. *Nat Commun*. 2019;10(1):1-10. doi:10.1038/s41467-019-10092-5

16. Day JN, Chau TTH, Wolbers M, et al. Combination antifungal therapy for cryptococcal meningitis. *N Engl J Med*. 2013;368(14):1291-1302. doi:10.1056/NEJMoa1110404

17. Day JN, Qihui S, Thanh LT, et al. Comparative genomics of *Cryptococcus neoformans* var. *grubii* associated with meningitis in HIV infected and uninfected patients in Vietnam. *PLoS Negl Trop Dis*. 2017;11(6):e0005628. doi:10.1371/journal.pntd.0005628

18. Lee A, Toffaletti DL, Tenor J, et al. Survival defects of *Cryptococcus neoformans* mutants exposed to human cerebrospinal fluid result in attenuated virulence in an experimental model of meningitis. *Infect Immun*. 2010;78(10):4213-4225. doi:10.1128/IAI.00551-10

19. Idnurm A, Walton FJ, Floyd A, Reedy JL, Heitman J. Identification of ENA1 as a virulence gene of the human pathogenic fungus *Cryptococcus neoformans* through signature-tagged insertional mutagenesis. *Eukaryot Cell*. 2009;8(3):315-326. doi:10.1128/EC.00375-08

20. Salas SD, Bennett JE, Kwon-Chung KJ, Perfect JR, Williamson PR. Effect of the laccase gene CNLAC1, on virulence of *Cryptococcus neoformans*. *J Exp Med*. 1996;184(August):377-386. doi:10.1084/jem.184.2.377

21. Eisenman HC, Mues M, Weber SE, et al. *Cryptococcus neoformans* laccase catalyses melanin synthesis from both D- and L-DOPA. *Microbiology*. 2007;153(12):3954-3962.

505 doi:10.1099/mic.0.2007/011049-0

506 22. Chen SC, Muller M, Zhou JZ, Wright LC, Sorrell TC. Phospholipase activity in *Cryptococcus*
507 *neoformans*: a new virulence factor? *J Infect Dis*. 1997;175(2):414-420.
508 doi:10.1093/infdis/175.2.414

509 23. Zaragoza O, Casadevall A. Experimental modulation of capsule size in *Cryptococcus*
510 *neoformans*. *Biol Proced Online*. 2004;6(1):10-15. doi:10.1251/bpo68

511 24. Hu G, Cheng P-Y, Sham A, Perfect JR, Kronstad JW. Metabolic adaptation in *Cryptococcus*
512 *neoformans* during early murine pulmonary infection. *Mol Microbiol*. 2008;69(6):1456-
513 1475. doi:10.1111/j.1365-2958.2008.06374.x

514 25. Levitz SM, Tabuni A, Nong SH, Golenbock DT. Effects of interleukin-10 on human
515 peripheral blood mononuclear cell responses to *Cryptococcus neoformans, Candida*
516 *albicans*, and lipopolysaccharide. *Infect Immun*. 1996;64(3):945-951.

517 26. Fang W, Fa Z, Liao W. Epidemiology of *Cryptococcus* and cryptococcosis in China. *Fungal*
518 *Genet Biol*. November 2014. doi:10.1016/j.fgb.2014.10.017

519 27. Khayhan K, Hagen F, Pan W, et al. Geographically structured populations of *Cryptococcus*
520 *neoformans* variety *grubii* in Asia correlate with HIV status and show a clonal population
521 structure. Zaragoza O, ed. *PLoS One*. 2013;8(9):e72222.
522 doi:10.1371/journal.pone.0072222

523 28. Chen M, Xu Y, Hong N, et al. Epidemiology of fungal infections in China. *Front Med*.
524 2018;12(1):58-75. doi:10.1007/s11684-017-0601-0

525 29. Dou H, Wang H, Xie S, Chen X, Xu Z, Xu Y. Molecular characterization of *Cryptococcus*
526 *neoformans* isolated from the environment in Beijing, China. *Med Mycol*. 2017;38:1-11.

527 doi:10.1093/mmy/myx026

528 30. Beale MA, Sabiiti W, Robertson EJ, et al. Genotypic diversity is associated with clinical
529 outcome and phenotype in cryptococcal meningitis across Southern Africa. Vinetz JM,
530 ed. *PLoS Negl Trop Dis*. 2015;9(6):e0003847. doi:10.1371/journal.pntd.0003847

531 31. Bojarczuk A, Miller KA, Hotham R, et al. *Cryptococcus neoformans* intracellular
532 proliferation and capsule size determines early macrophage control of infection. *Sci Rep*.
533 2016;6(October 2015):21489. doi:10.1038/srep21489

534 32. Zaragoza O, Chrisman CJ, Castelli MV, et al. Capsule enlargement in *Cryptococcus*
535 *neoformans* confers resistance to oxidative stress suggesting a mechanism for
536 intracellular survival. *Cell Microbiol*. 2008;10(10):2043-2057. doi:10.1111/j.1462-
537 5822.2008.01186.x

538 33. García-Rodas R, Casadevall A, Rodríguez-Tudela JL, Cuenca-Estrella M, Zaragoza O.
539 *Cryptococcus neoformans* capsular enlargement and cellular gigantism during *Galleria*
540 *mellonella* infection. *PLoS One*. 2011;6(9):e24485. doi:10.1371/journal.pone.0024485

541 34. Robertson EJ, Najjuka G, Rolfes M a, et al. *Cryptococcus neoformans* ex vivo capsule size
542 is associated with intracranial pressure and host immune response in HIV-associated
543 cryptococcal meningitis. *J Infect Dis*. 2014;209(1):74-82. doi:10.1093/infdis/jit435

544 35. Vecchiarelli A, Pericolini E, Gabrielli E, et al. *Cryptococcus neoformans* galactoxylomannan
545 is a potent negative immunomodulator, inspiring new approaches in anti-inflammatory
546 immunotherapy. *Immunotherapy*. 2011;3:997-1005. doi:10.2217/imt.11.86

547 36. Kronstad J, Saikia S, Nielson ED, et al. Adaptation of *Cryptococcus neoformans* to
548 mammalian hosts: integrated regulation of metabolism and virulence. *Eukaryot Cell*.

2012;11(2):109-118. doi:10.1128/EC.05273-11

37. Botts MR, Giles SS, Gates MA, Kozel TR, Hull CM. Isolation and characterization of *Cryptococcus neoformans* spores reveal a critical role for capsule biosynthesis genes in spore biogenesis. *Eukaryot Cell*. 2009;8(4):595-605. doi:10.1128/EC.00352-08

38. Bódi Z, Farkas Z, Nevozhay D, et al. Phenotypic heterogeneity promotes adaptive evolution. *PLoS Biol*. 2017;15(5):e2000644. doi:10.1371/journal.pbio.2000644

39. Chow EWL, Morrow CA, Djordjevic JT, Wood IA, Fraser JA. Microevolution of *Cryptococcus neoformans* driven by massive tandem gene amplification. *Mol Biol Evol*. 2012;29(8):1987-2000. doi:10.1093/molbev/mss066

40. Fernandes KE, Brockway A, Haverkamp M, et al. Phenotypic variability correlates with clinical outcome in *Cryptococcus* isolates obtained from Botswanan HIV/AIDS Patients. *MBio*. 2018;9(5):e02016-18. doi:10.1128/mBio.02016-18

41. Zaragoza O, Alvarez M, Telzak A, Rivera J, Casadevall A. The relative susceptibility of mouse strains to pulmonary *Cryptococcus neoformans* infection is associated with pleiotropic differences in the immune response. *Infect Immun*. 2007;75(6):2729-2739. doi:10.1128/IAI.00094-07

42. Cheng P-Y, Sham A, Kronstad JW. *Cryptococcus gattii* isolates from the British Columbia cryptococcosis outbreak induce less protective inflammation in a murine model of infection than *Cryptococcus neoformans*. *Infect Immun*. 2009;77(10):4284-4294. doi:10.1128/IAI.00628-09

43. Sellers RS, Clifford CB, Treuting PM, Brayton C. Immunological variation between inbred laboratory mouse strains: points to consider in phenotyping genetically immunomodified

mice. *Vet Pathol*. 2012;49(1):32-43. doi:10.1177/0300985811429314

44. Lortholary O, Improvisi L, Rayhane N, et al. Cytokine profiles of AIDS patients are similar to those of mice with disseminated *Cryptococcus neoformans* infection. *Infect Immun*. 1999;67(12):6314-6320.

45. Jain A V, Zhang Y, Fields WB, et al. Th2 but not Th1 immune bias results in altered lung functions in a murine model of pulmonary *Cryptococcus neoformans* infection. *Infect Immun*. 2009;77(12):5389-5399. doi:10.1128/IAI.00809-09

46. Koguchi Y, Kawakami K. Cryptococcal infection and Th1-Th2 cytokine balance. *Int Rev Immunol*. 2002;21(4-5):423-438. doi:10.1080/08830180190048109

47. Chaka W, Verheul AF, Vaishnav V V, et al. *Cryptococcus neoformans* and cryptococcal glucuronoxylomannan, galactoxylomannan, and mannoprotein induce different levels of tumor necrosis factor alpha in human peripheral blood mononuclear cells. *Infect Immun*. 1997;65(1):272-278.

48. Levitz SM, Tabuni A, Kornfeld H, Reardon CC, Golenbock DT. Production of tumor necrosis factor alpha in human leukocytes stimulated by *Cryptococcus neoformans*. *Infect Immun*. 1994;62(5):1975-1981.

49. García-Rivera J, Casadevall A. Melanization of *Cryptococcus neoformans* reduces its susceptibility to the antimicrobial effects of silver nitrate. *Med Mycol*. 2001;39:353-357. doi:10.1080/mmy.39.4.353.357

593

594

595

596 **FIGURE LEGENDS**

597 **Figure 1. *In vitro* induced capsule thickness and cell diameter of individual *Cryptococcus***

598 ***neoformans* strains from Vietnam:** Cells were grown on DMEM medium/5% CO_2 and visually

599 assessed by India ink staining. Images were taken for single cells measurement using ImageJ

600 software. Capsule thickness is obtained by subtracting cell body diameter from total cell

601 diameter. AFLP-VNI-γ/MLST-ST5 strains expressed higher degree of variation in both capsule

602 size and cell diameter *in vitro,* which remains significant even when the outlier BMD1646 was

603 removed from the analysis (p<0.0001 for both capsule and cell size, Fligner-Killeen test).

604 Scattered plot represents single cells from an individual strain. Data for individual strains are

605 presented as mean with error bars denoting standard deviation. Strains selected for experiment

606 in mice were indicated by asterisks.

607

608 **Figure 2. Kaplan-Meier survival curves for mice infected with either ST5 (n = 5) or non-ST5 (n=**

609 **3) *Cryptococcus neoformans* strains**. 10 A/J mice were infected per strain (five ST5 strains and

610 three non-ST5 strains). Mice were monitored daily until the point of more than 15% weight loss

611 or visible suffering and were then sacrificed by CO_2 inhalation. Mice infected with ST5 strains

612 had statistically significantly longer survival times than those infected with non-ST5 strains

613 (P<0.0001, Mantel-Cox log rank test) (Panel A). Two ST5 strains, BK147 and BMD1646, were

614 attenuated, suggesting high degree of heterogeneity within the ST5 cluster. Mice infected with

615 BK147 and BMD1646 survived for as long as 42 days post-infection, at which point the
616 experiment was terminated and all infected mice sacrificed (Panel B).

617

618 **Figure 3. Fungal burden in mouse lung and brain tissue at days 7, 14 and the point of**
619 **impending death (mortality experiment) according to infecting genotype.** *In vivo* virulence
620 (tissue fungal burden and mortality) was assessed in three independent mouse infection
621 experiments. In the first two experiments, five A/J mice were infected with each of the eight
622 test *C. neoformans* isolate (five ST5 isolates and 3 non-ST5 isolates, total N=40 mice in each
623 experiment). All mice were sacrificed at day 7 post-infection in the first experiment and at day
624 14 post-infection in the second experiment to assess *in vivo* fungal burden in mouse lung and
625 brain. Fungal burden in the lung and brain at either day 7 or day 14 for each isolate is presented
626 in panel A. In the last experiment, ten A/J mice were infected with each of the 8 test *C.*
627 *neoformans* isolate (five ST5 isolates and 3 non-ST5 isolates, N=80 mice in total) and monitored
628 daily until the point when 15% of body weight loss, a sign of distress and impending death, was
629 evident. Fungal burden in lung and brain at point of death was again assessed as before. Here,
630 for each strain, five mice were randomly selected from the ten test mice for fungal burden
631 investigation. The pooled fungal burden in non-ST5 infections was higher than in ST5 infections
632 in both lung tissue at all time points, and in brain tissue at the point of sacrifice (Panel B) (For P
633 values see text). Boxplots (Tukey's method) describe the median and interquartile range, the
634 whiskers demarcate the largest or smallest values that were not outliers (black dots); outliers
635 are defined as more than 1.5 times the interquartile range from the nearest quartile.

Figure 4. Genotype-specific cytokine concentrations from lung homogenate of A/J mice at 7 and 14 days post infection with 5x10^4 *C. neoformans* cells/mouse. Five mice were infected with each strain from each genotype at each time points. ST5 strains induced significantly higher levels of TNF-α at day 7, suggesting an earlier and more profound initial inflammatory response in infected mice. By day 14 mice infected with non-ST5 strains have higher levels proinflammatory cytokines, probably a result of ST5 yeasts being cleared more rapidly from infected mice. The horizontal line within the box indicates the median; boundaries of the box indicate the 25th and 75th percentile and the whiskers indicate the highest and lowest values of the results; outliers are denoted as black dots (Tukey's method). Data are standardized as picograms of cytokine per gram lung tissue. Asterisks indicate statistically significant differences (Mann-Whitney test).

Figure 5. Genotype-specific changes in cytokine concentrations from lung homogenate of A/J mice infected with *C. neoformans* between day 7 and day 14 post-infection. Box and whisker plots (Tukey's method) compare levels of each cytokine between day 7 and day 14 for each genotype. Data are standardized as picograms of cytokine per gram lung tissue. Asterisks indicate statistically significant differences (Mann-Whitney test).

Figure 6. Periodic Acid Schiff (PAS) staining of pulmonary tissue from mice infected with BMD1338 and BMD1415 on days 7 and 14. The two strains represent ST5 and non-ST5, respectively. A/J mice were inoculated intranasally with 5x10^4 yeast cells. Lung specimens were

harvested at days 7 and 14 for histopathological examination. Photomicrographs were obtained at 200X magnification; the scale bar represents 215 µm). (A-B): lung sections from mice infected with BMD1338 (VNI-γ/ST5) at day 7 and day 14, respectively. (C-D): lung sections from mice infected with BMD1415 (VNI-δ/ST4) at day 7 and day 14, respectively. Perivascular infiltration (red arrows) and necrosis are more marked by day 14 for both strains. Encapsulated yeasts (yellow arrows), notable for the larger cell size and capsule thickness of BMD 1338 compared with BMD1415.

Figure 7. Mucicarmine staining of capsular material in paraffin-embedded mice pulmonary tissue.

Uninflated lung specimens were harvested from mice as described in the methods. Mucicarmine staining was performed to visualize the cryptococcal capsule. Photomicrographs were captured at 400X magnification with scale bar indicating 55µm. Capsular polysaccharide is stained pink (indicated by blue arrows), demonstrating diffuse localization consistent with extensive capsule production by yeasts in the alveolar space.

FIGURE S1. Phenotyping of *C. neoformans* var. *grubii* isolates from Vietnam (ST5: n=15 and non-ST5: n=15). Data were obtained from 30 isolates (15 ST5 and 15 non-ST5) in 3 different experiment batches, with 3 technical replicates of each isolate per batch. Data are expressed as the ratio between measurements of the test isolates and that of H99. Boxplots (Tukey's method) describe the median and interquartile range (panel A-C). For assessment of urease activity (panel D), we used the time to complete color change of the agar plate as an indirect measure of extracellular urease activity since all *C. neoformans* var. *grubii* isolates in our

collection were positive for urease activity. Each isolate were tested in triplicate and monitored in real time by live-imaging. No significant difference in any virulence-associated phenotype were observed between the two MLST groups.

FIGURE S2. Growth at different temperature of 8 *C. neoformans* (five ST5 and three non-ST5) isolates from Vietnamese patients used in the murine infection experiments. All strains expressed similar growth at 30°C. Two ST5 isolates (BMD1646 and BK147) displayed diminished growth at 37°C compared to other test isolates.

FIGURE S3. ***Ex vivo* growth in human cerebrospinal fluid (CSF) of 8 clinical *C. neoformans* isolates from Vietnamese patients that were tested for virulence in mice, representing both ST5 (n = 5) and non-ST5 (n = 3) genotypes**. The same inoculum of yeasts were inoculated in pooled human CSF and incubated at 37°C. The inoculated CSF was serially diluted and plated on YPD agar at day 1 and day 3 post-inoculation. The wild-type H99 strain and the H99-derived mutant *Δena1*, lacking a cation ATPase transporter which results in decreased viability in human CSF and within macrophages, were included as controls. An apparent difference in growth between ST5 and non-ST5 isolates could be observed at day 3.

FIGURE S4. Melanin production on L-DOPA medium of eight clinical *C. neoformans* isolates from Vietnamese patients representing both S5 (n =5) and non-ST5 (n = 3) genotypes that were tested for virulence in mice. For each isolates, 10µl of 10^6 cell suspension was inoculated on L-DOPA agar and incubated in the dark at 30°C and 37°C. No clear genotype-specific patterns of melanization were observed at either 30°C or 37°C. The five ST5 strains displayed marked

variation in the degree of pigment production, from mildly melanized (BK147) to highly melanized (BK44 and BMD1646).

FIGURE S5: **Histopathological scores across 4 categories of tissue damage (Inflammation, necrosis, hemorrhage and edema).** Thin sections of paraffin-embedded lung specimens from infected mice were stained using the Periodic Acid Schiff (PAS) method. Specimens were assessed by an independent pathologist who was blind to infecting isolate and in randomized order. Scores ranged from 0 (no changes) to 10 (severe changes), corresponding to the severity of pathology in in each category as per the Duke Veterinary Diagnostic Laboratory protocol (Division of Laboratory Animal Resources).

721 **TABLES**

722 **TABLE 1** *Cryptococcus neoformans* isolate clinical source and typing (n=30).

Isolate data				Patient data	
Order	Strain name	WGS cluster	MLST sequence type	Underlying Disease	Sex
1	BK14	VNIa-4	4	HIV	M
2	BK163	VNIa-4	4	HIV	M
4	BK225	VNIa-4	4	HIV	M
6	BK48	VNIa-4	4	HIV	M
7	BK59	VNIa-4	4	HIV	F
8	BK69	VNIa-4	4	HIV	M
9	BK74	VNIa-4	4	HIV	M
10	BK80*	VNIa-4	4	HIV	M
11	BK87	VNIa-4	4	HIV	M
12	BK88	VNIa-4	4	HIV	M
13	BK89	VNIa-4	4	HIV	M
15	BMD1415*	VNIa-4	4	Lupus	M
3	BK218	VNIa-4	6	HIV	M
5	BK234	VNIa-4	6	HIV	F
14	BMD1367*	VNIa-4	306	Gastric cancer	F

16	BK147*	VNIa-5	5	HIV	M
17	BK44*	VNIa-5	5	HIV	M
18	BMD101	VNIa-5	5	None known	M
19	BMD1228	VNIa-5	5	None known	F
20	BMD1291	VNIa-5	5	None known	F
21	BMD1338*	VNIa-5	5	None known	M
22	BMD1353	VNIa-5	5	None known	M
23	BMD1452	VNIa-5	5	None known	F
24	BMD1646*	VNIa-5	5	None known	M
25	BMD1716	VNIa-5	5	None known	F
26	BMD367	VNIa-5	5	None known	M
27	BMD673	VNIa-5	5	None known	F
28	BMD700*	VNIa-5	5	None known	M
29	BMD854	VNIa-5	5	None known	F
30	BMD899	VNIa-5	5	None known	F

WGS = whole genome sequencing

MLST = multi locus sequence typing

M = Male, F = Female

** indicates isolates selected for mouse experiment*

723

724

725 **TABLE 2** Variability in *in vitro* capsule thickness and cell diameter of *Cryptococcus neoformans*

726 strains by Sequence Type (ST)

727

	MLST Group	
Variable	**ST5**	**Non-ST5**
Capsule Thickness (µm)		
Mean*	2.64	2.01
95% CI	2.49 - 2.79	1.94 - 2.07
Range	0.01 - 9.56	0.02 - 6.16
Coefficient of Variation[$]		
(%)	0.63	0.37
Cell diameter (µm)		
Mean*	11.38	9.69
95% CI of Mean	10.96 - 11.79	9.52 - 9.87
Range	4.74 - 27.22	5.25 - 19.89
Coefficient of Variation[$]		
(%)	0.41	0.20

728 ** P<0.0001, t-test with Welch's correction.*

729 [$] *P< 0.0001, Fligner-Killeen test of homogeneity of variance.*

730

731

732 **TABLE 3** Tissue fungal burden in lung and brains of mice at days 7, 14 and at time of death by

733 infecting MLST Sequence Type (ST)

	Fungal burden (Mean $\log_{10}$ colony forming units per gram of tissue) [95%CI]		
Tissue	**ST5**	**Non-ST5**	**P Value**
Lung (Day 7)	4.96 [3.86 - 6.05]	7.07 [6.85 - 7.29]*	<0.001
Brain (Day 7)	0.81 [0.38 - 1.24]	1.59 [0.87 - 2.30]	0.054
Lung (Day 14)	5.48 [4.34 - 6.62]	8.00 [7.77 - 8.23]*	<0.0001
Brain (Day 14)	1.56 [0.81 - 2.31]	1.91 [1.12 - 2.69]	0.36
Lung (Death)	3.81 [3.05 - 4.57]	6.53 [6.30 - 6.76]*	<0.0001
Brain (Death)	2.90 [2.23 - 3.56]	4.29 [3.90 - 4.68]*	0.01

**Mann-Whitney test.*

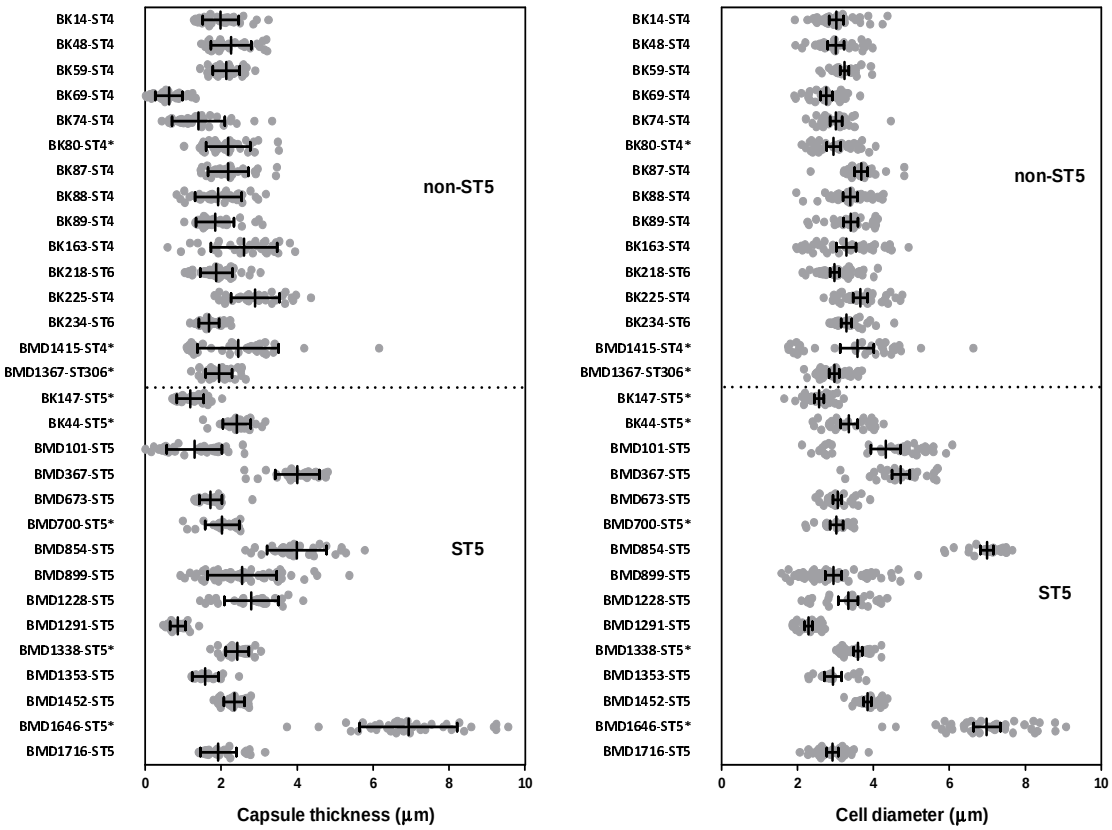

734

735 **Figure 2. *In vitro* induced capsule thickness and cell diameter of individual *Cryptococcus neoformans* strains from Vietnam:** Cells were grown

736 on DMEM medium/5% CO_2 and visually assessed by India ink staining. Images were taken for single cells measurement using ImageJ software.

737 Capsule thickness is obtained by subtracting cell body diameter from total cell diameter. AFLP-VNI-γ/MLST-ST5 strains expressed higher degree
738 of variation in both capsule size and cell diameter *in vitro*, which remains significant even when the outlier BMD1646 was removed from the
739 analysis (p<0.0001 for both capsule and cell size, Fligner-Killeen test). Scattered plot represents single cells from an individual strain. Data for
740 individual strains are presented as mean with error bars denoting standard deviation. Strains selected for experiment in mice were indicated by
741 asterisks.

742

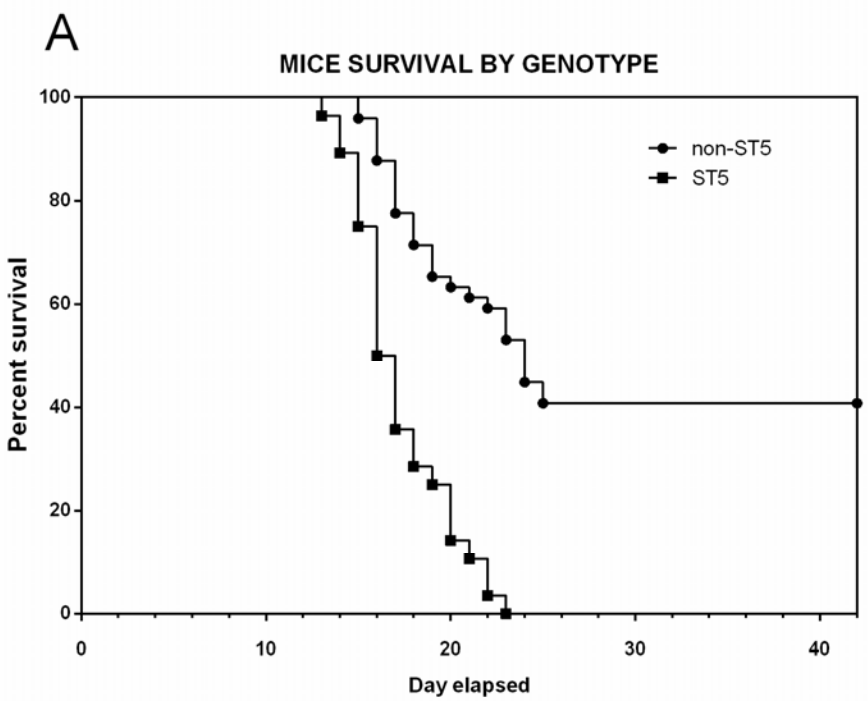

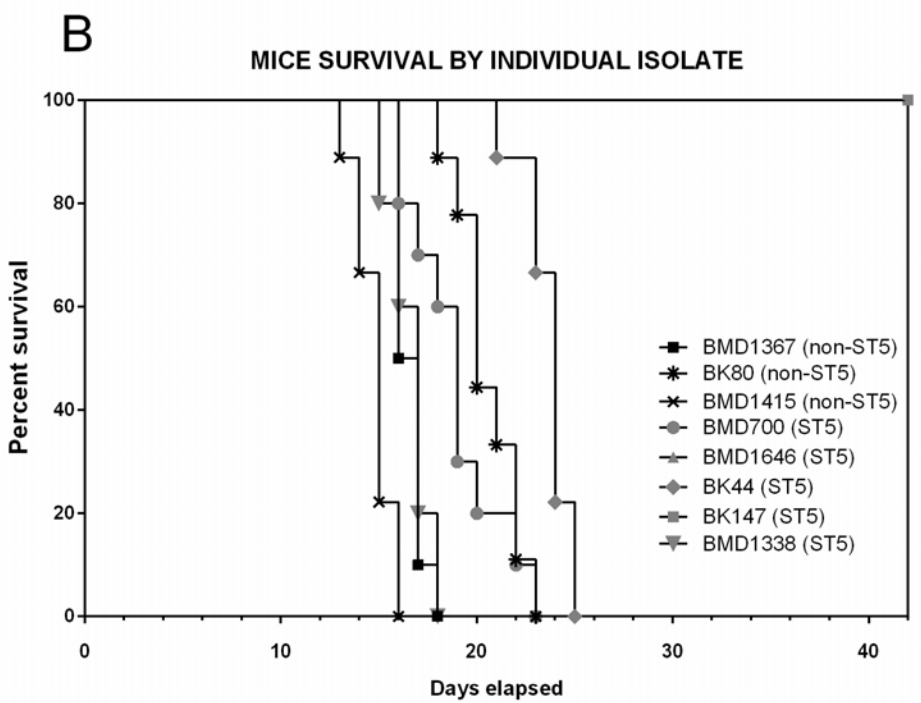

744 **Figure 2. Kaplan-Meier survival curves for mice infected with either ST5 (n = 5) or non-ST5 (n= 3) *Cryptococcus neoformans* strains**. 10
745 A/J mice were infected per strain (five ST5 strains and three non-ST5 strains). Mice were monitored daily until the point of more than 15%
746 weight loss or visible suffering and were then sacrificed by CO_2 inhalation. Mice infected with ST5 strains had statistically significantly longer
747 survival times than those infected with non-ST5 strains ($P<0.0001$, Mantel-Cox log rank test) (Panel A). Two ST5 strains, BK147 and
748 BMD1646, were attenuated, suggesting high degree of heterogeneity within the ST5 cluster. Mice infected with BK147 and BMD1646 survived
749 for as long as 42 days post-infection, at which point the experiment was terminated and all infected mice sacrificed (Panel B).

750

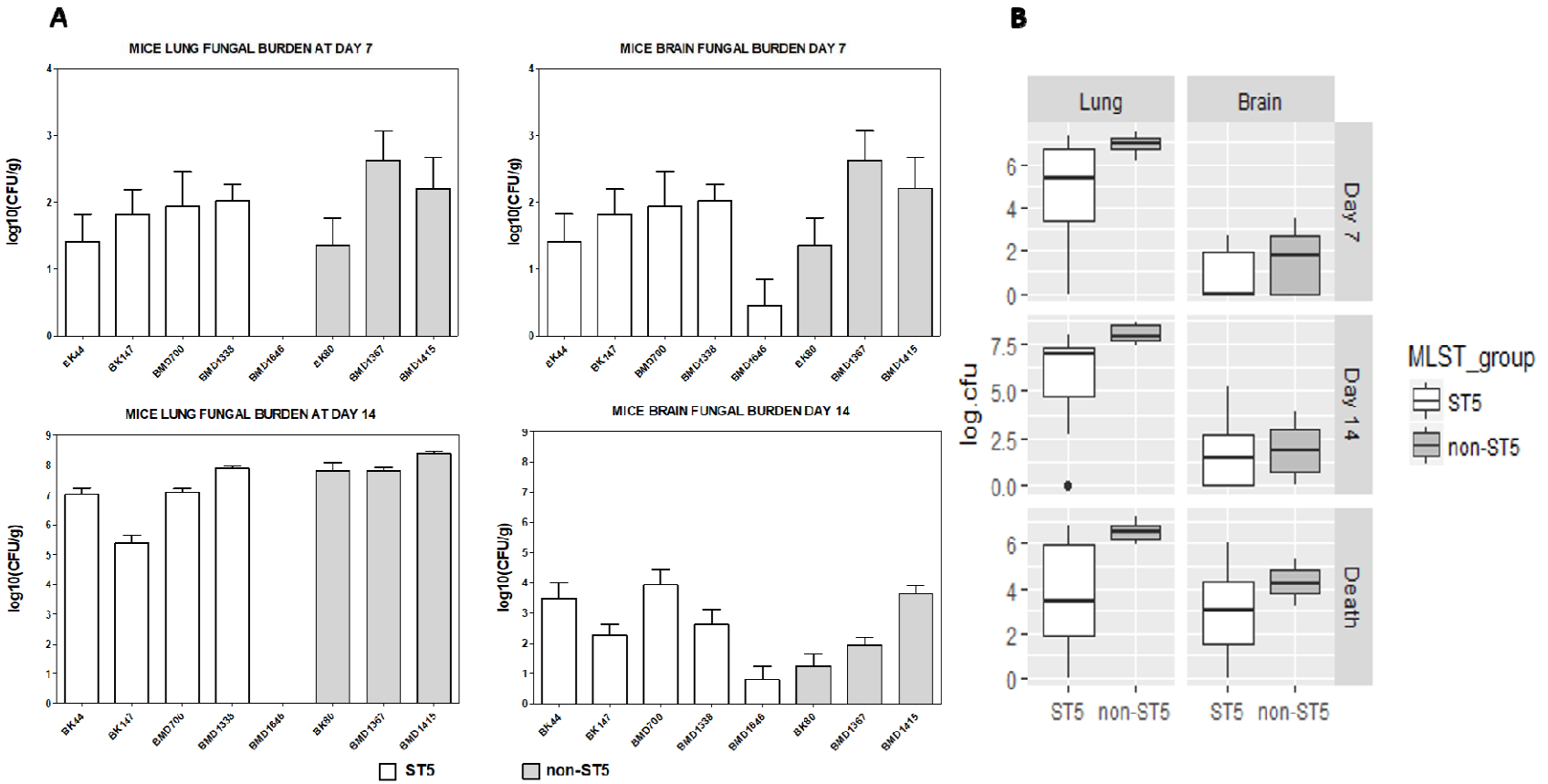

Figure 3. Fungal burden in mouse lung and brain tissue at days 7, 14 and the point of impending death (mortality experiment) according to infecting genotype. *In vivo* virulence (tissue fungal burden and mortality) was assessed in three independent mouse infection experiments. In the first two experiments, five A/J mice were infected with each of the eight test *C. neoformans* isolates (five ST5 isolates and 3 non-ST5 isolates,

total N=40 mice in each experiment). All mice were sacrificed at day 7 post-infection in the first experiment and at day 14 post-infection in the second experiment to assess *in vivo* fungal burden in mouse lung and brain. Fungal burden in the lung and brain at either day 7 or day 14 for each isolate is presented in panel A. In the last experiment, ten A/J mice were infected with each of the 8 test *C. neoformans* isolate (five ST5 isolates and 3 non-ST5 isolates, N=80 mice in total) and monitored daily until the point when 15% of body weight loss, a sign of distress and impending death, was evident. Fungal burden in lung and brain at point of death was again assessed as before. Here, for each strain, five mice were randomly selected from the ten test mice for fungal burden investigation. The pooled fungal burden in non-ST5 infections was higher than in ST5 infections in both lung tissue at all time points, and in brain tissue at the point of sacrifice (Panel B) (For P values see text). Boxplots (Tukey's method) describe the median and interquartile range, the whiskers demarcate the largest or smallest values that were not outliers (black dots); outliers are defined as more than 1.5 times the interquartile range from the nearest quartile.

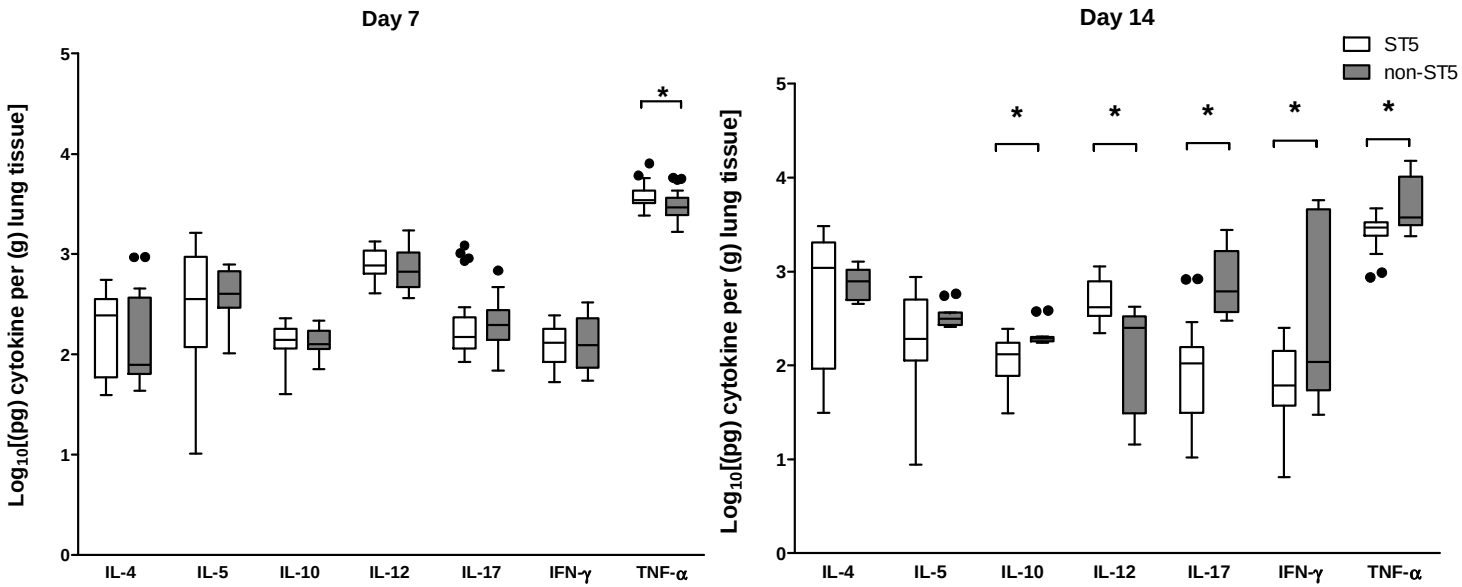

765

766

767 **Figure 4. Genotype-specific cytokine concentrations from lung homogenate of A/J mice at 7 and 14 days post infection with 5x10^4 *C.***

768 ***neoformans* cells/mouse.** Five mice were infected with each strain from each genotype at each time points. ST5 strains induced significantly

769 higher levels of TNF-α at day 7, suggesting an earlier and more profound initial inflammatory response in infected mice. By day 14 mice infected

770 with non-ST5 strains have higher levels proinflammatory cytokines, probably a result of ST5 yeasts being cleared more rapidly from infected

771 mice. The horizontal line within the box indicates the median; boundaries of the box indicate the 25th and 75th percentile and the whiskers

indicate the highest and lowest values of the results; outliers are denoted as black dots (Tukey's method). Data are standardized as picograms of cytokine per gram lung tissue. Asterisks indicate statistically significant differences (Mann-Whitney test).

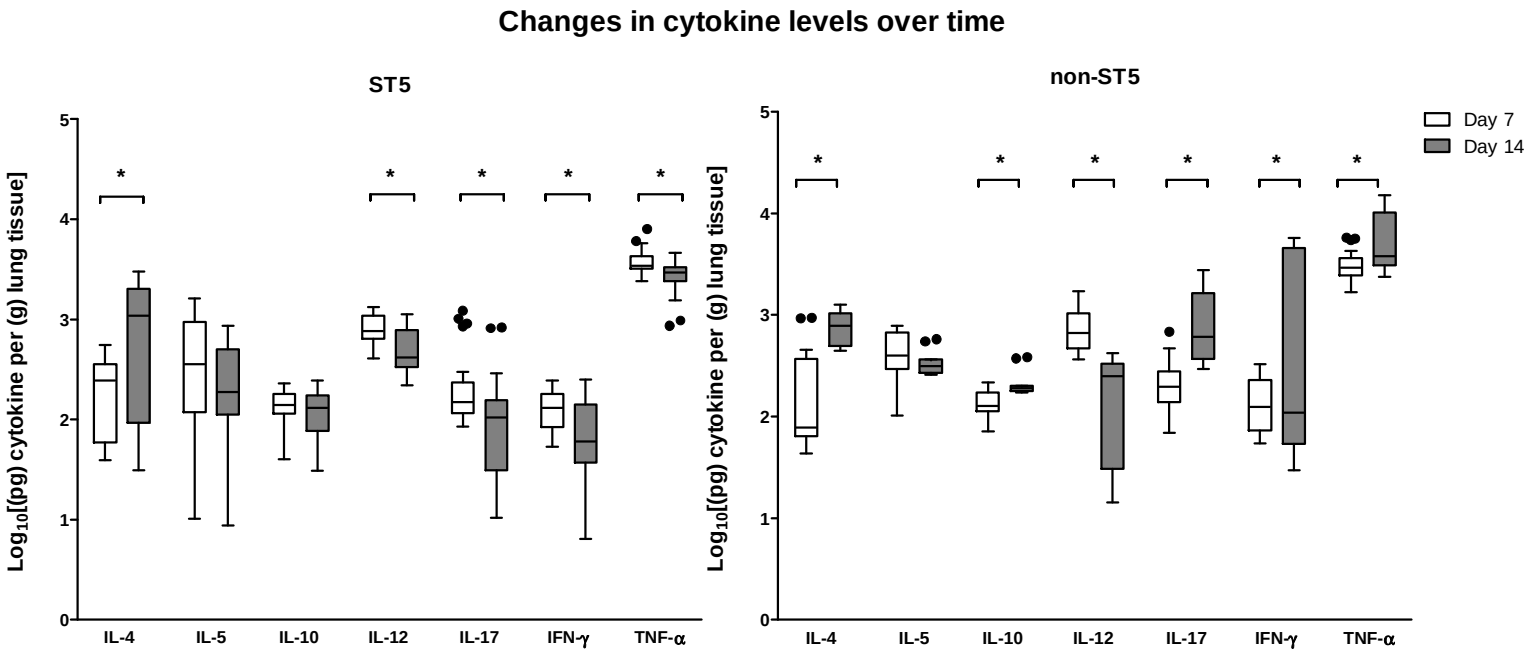

Figure 5. Genotype-specific changes in cytokine concentrations from lung homogenate of A/J mice infected with *C. neoformans* between day 7 and day 14 post-infection. Box and whisker plots (Tukey's method) compare levels of each cytokine between day 7 and day 14 for each genotype. Data are standardized as picograms of cytokine per gram lung tissue. Asterisks indicate statistically significant differences (Mann-Whitney test).

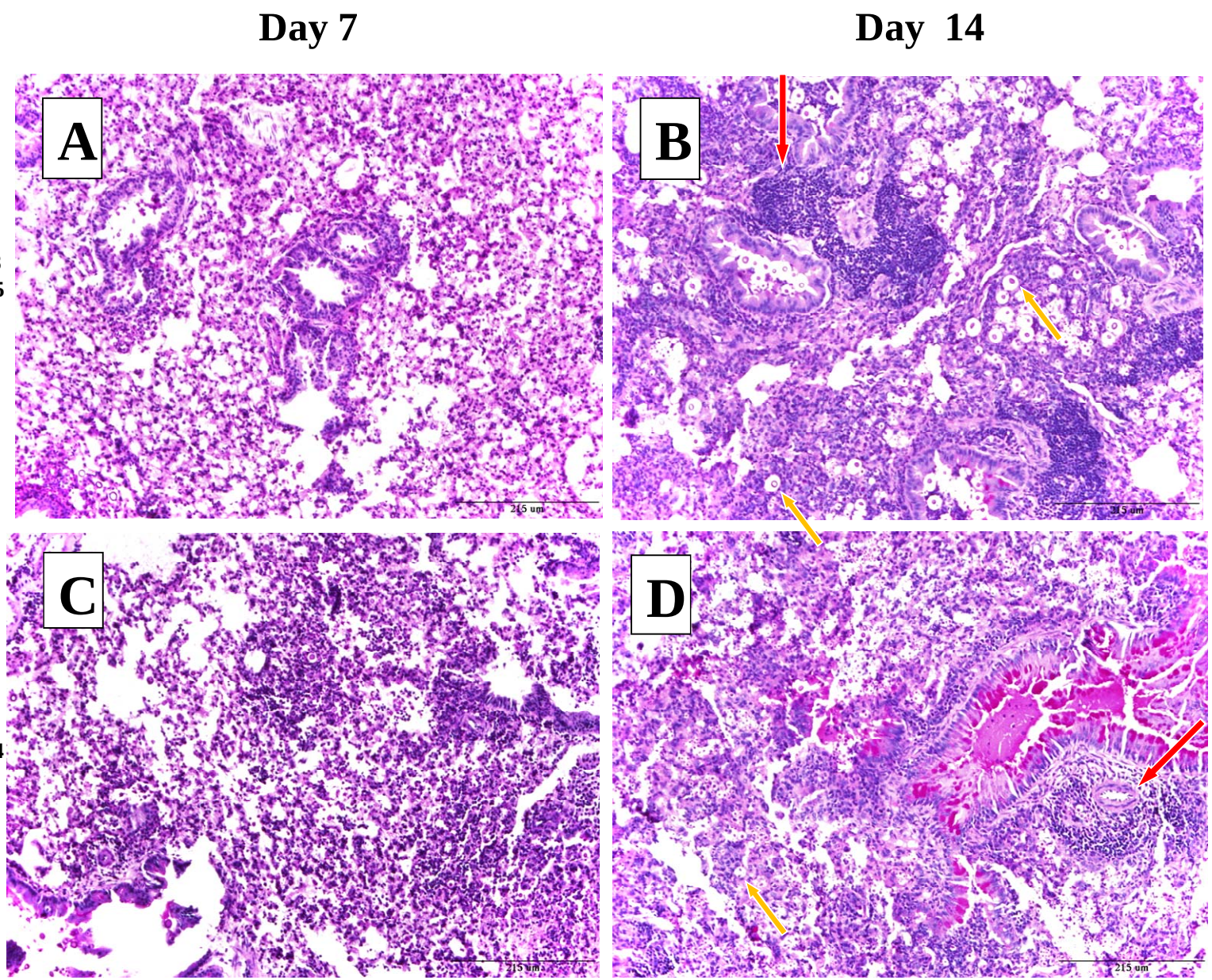

782

Figure 6. Periodic Acid Schiff (PAS) staining of pulmonary tissue from mice infected with BMD1338 and BMD1415 on days 7 and 14. The two strains represent ST5 and non-ST5, respectively. A/J mice were inoculated intranasally with $5x10^4$ yeast cells. Lung specimens were harvested at days 7 and 14 for histopathological examination. Photomicrographs were obtained at 200X magnification; the scale bar represents 215 µm). (A-B): lung sections from mice infected with BMD1338 (VNI-γ/ST5) at day 7 and day 14, respectively. (C-D): lung sections from mice infected with BMD1415 (VNI-δ/ST4) at day 7 and day 14, respectively. Perivascular infiltration (red arrows) and necrosis are more marked by day 14 for both strains. Encapsulated yeasts (yellow arrows), notable for the larger cell size and capsule thickness of BMD 1338 compared with BMD1415.

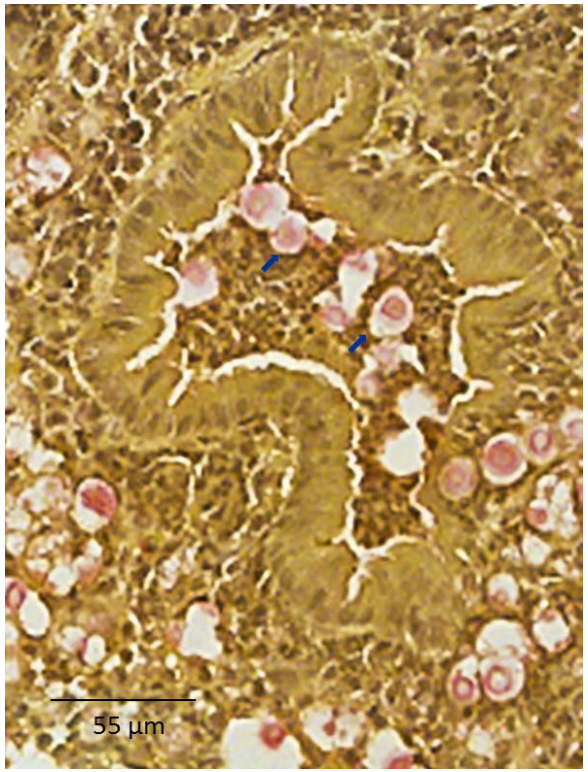

Figure 7. Mucicarmine staining of capsular material in paraffin-embedded mice pulmonary tissue.

Uninflated lung specimens were harvested from mice as described in the methods. Mucicarmine staining was performed to visualize the cryptococcal capsule. Photomicrographs were captured at 400X magnification with scale bar indicating 55µm. Capsular polysaccharide is stained pink (indicated by blue arrows), demonstrating diffuse localization consistent with extensive capsule production by yeasts in the alveolar space.

800

801